

pubs.acs.org/cm Article

Effects of Electronic Coupling on Bright and Dark Excitons in a 2D Array of Strongly Confined CsPbBr₃ Quantum Dots

Xueting Tang, Daniel Rossi, Jinwoo Cheon, and Dong Hee Son*



Cite This: Chem. Mater. 2022, 34, 7181-7189



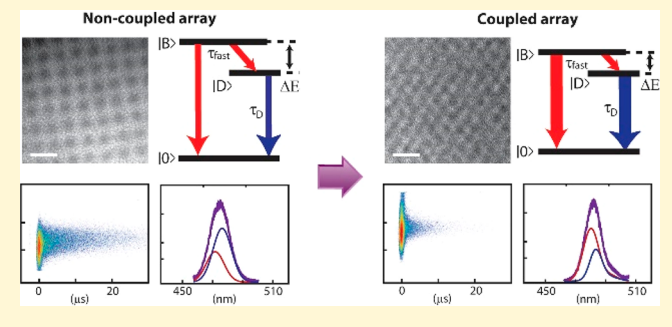
ACCESS I

III Metrics & More

Article Recommendations

SI Supporting Information

ABSTRACT: In contrast to the weakly confined quantum dots dominated by bright excitons, strongly quantum confined CsPbBr₃ QDs exhibit both bright and dark exciton photoluminescence (PL) at cryogenic temperatures, making them a unique source of photons and charges of two very different natures. Here, we investigate the effect of inter-QD electronic coupling on the relative energetics and dynamics of the bright and dark excitons, which dictate the PL properties of the coupled arrays of these QDs at low temperatures. For this purpose, we fabricated 2D closepacked arrays of NaBr-passivated CsPbBr₃ QDs with a subnanomter facet-to-facet distance, which was necessary to introduce



electronic coupling. In addition to the redshift of the PL due to electronic coupling, the electronically coupled array of strongly confined CsPbBr₃ QDs exhibited narrowed bright—dark level splitting and an acceleration of the decay of both bright and dark exciton PL at cryogenic temperatures. These observations are qualitatively analogous to the effects of increasing the volume of noninteracting QDs, which can be explained by the delocalization of exciton wave function among the coupled QDs.

■ INTRODUCTION

Exciton properties of noninteracting colloidal quantum dots (QDs) of a given material are dictated by the spatial distribution and electronic interactions of electrons and holes, which are dependent on the size, shape, surface ligands, and surrounding medium of the QDs. When the QDs are sufficiently close together, overlap of exciton wave functions or increased dipolar interactions between the QDs can alter level structure and dynamics of the exciton via electronic coupling or interparticle energy or charge transfer. 1-4 This results in the photophysical properties of an interacting ensemble of QDs being different from those of the isolated QDs, for example, the redshift of the exciton transition energy^{3,5-8} and increased electrical conductivity 9-13 observed in a densely packed film of QDs. To bring the QDs close enough to strengthen the interparticle interactions, 2D and 3D arrays of QDs are often created after the long-chain organic ligands typically used to passivate the surface of the QDs are replaced with shorter ones. 11,13,14 In some cases, directly connected QD dimers were created to introduce electronic coupling between the QDs, which gives rise to the properties of two coupled excitons. ^{4,15,16}

Earlier studies on the properties of 2D and 3D array of QDs were performed mostly with II–VI and IV–VI QDs and focused on enhancing their properties for light-emitting and photovoltaic applications. ^{1,17} More recently, the interest in the role of electronic or dipolar coupling in the QD arrays expanded into lead halide perovskite (LHP) nanocrystals (NCs), which have emerged as a superior alternative to many existing semiconductor QDs in these applications. ^{18,19} Several

recent studies on the 3D superlattices of LHP NCs reported the observation of superfluorescence and a change in the incoherent exciton emission propagated through the superlattice.^{20–24} However, most of these studies on the array of LHP NCs were performed with weakly or nonconfined NCs passivated with long-chain ligands; therefore, interparticle interactions were relatively weak in these systems. Recent synthetic progress enabled the production of strongly quantum-confined LHP QDs with high uniformity, which was previously difficult to obtain.²⁵ These QDs also exhibit quite different exciton properties from those of their weakly or nonconfined counterparts. For instance, strongly quantum confined CsPbX₃ QDs exhibit intense and microsecond-lived photoluminescence (PL) from dark excitons at low temperatures, in contrast to weakly confined QDs whose PL is dominated by bright excitons. 26 Therefore, strong confinement in LHP QDs not only facilitates interparticle electronic coupling by increasing the wave function overlap but also gives access to dark excitons that may function as either the source of a photon or charge or a quantum information carrier that can benefit from its longevity.

Received: March 4, 2022 Revised: July 18, 2022 Published: August 1, 2022





To this end, we created well-ordered 2D arrays of strongly quantum confined CsPbBr3 QDs with a facet-to-facet distance of several angstroms (Å) and investigated the effect of electronic coupling on the energetics and dynamics of bright and dark excitons. For this purpose, we employed a ligand exchange method to replace the surface-bound long-chain organic ligand with NaBr, which can create 2D arrays of QDs with a lower facet-to-facet distance of ~ 5 Å. ²⁷ Using spectrally and temporally resolved measurements of the PL at varying temperatures (5-300 K), we investigated how electronic coupling altered the level structure and relaxation dynamics of bright and dark excitons in strongly confined CsPbBr₃ QDs. Results from the present study will be important for utilizing electronically coupled LHP QDs in the strongly confined regime, where both bright and dark excitons are accessible as the source of photons or charges.

EXPERIMENTAL SECTION

Synthesis of CsPbBr₃ QDs. Strongly quantum confined CsPbBr₃ QDs were synthesized following a previously published procedure, which is briefly described below. ²⁵ The Cs precursor was prepared by dissolving Cs₂CO₃ (0.25 g) in a mixture of oleic acid (OA, 0.8 g) and 1-octadecene (ODE, 7 g) at 130 °C under N2 atmosphere on a Schlenk line after the solvent was degassed at room temperature for 10 min under vacuum. The Pb/Br precursor was prepared by dissolving PbBr₂ (190 mg) and ZnBr₂ (500 mg) in the mixture of ODE (6 mL), OA (3.2 mL) and oleyl amine (OAm, 3.2 mL), and the reaction mixture was heated at 120 °C under vacuum for 5 min. The reaction was initiated by injecting 2 mL of the Cs precursor solution into the Pb/Br precursor solution under N2 atmosphere at a chosen reaction temperature to obtain the QDs of different sizes (80 °C for 3.8 nm QDs, 120 °C for 4.2 nm QDs, and 160 °C for 5.3 nm QDs). After ~3 min of reaction, the product was cooled to room temperature. After allowing the remaining excess reactant to precipitate at room temperature, the product mixture was centrifuged, and the QDs were recovered from the supernatant. The removal of the remaining excess reactant via precipitation from the supernatant containing QDs were repeated several times. The recovered QDs were purified by precipitating them with acetone and redispersing them in hexane.

Ligand Replacement from Oleylammonium Bromide (OLAB) to NaBr. The ligand replacement from OLAB to NaBr was performed using a procedure modified from the previously published method, which involved sequential two-step exchange.²⁷ Two ligand precursor solutions were prepared for this purpose: phenylethylammonium bromide (PEAB, 250 mg) in 1 mL of anhydrous DMF and NaBr (100 mg) in 1 mL of anhydrous DMF. Initially, the concentrated OLAB-passivated QD solution in hexane (300 µL, 0.8 mM) was precipitated with methyl acetate and redispersed in toluene three times. This partially removed the OLAB ligand, resulting in a loss of the PL intensity. Subsequently, 10 μ L of the PEAB solution in DMF was added to the QD solution, and the reaction mixture was mixed vigorously. After the precipitated excess PEAB salt was removed by centrifugation, the addition of the PEAB solution and the removal of excess PEAB were repeated three more times. At this stage, the PL intensity of the QD solution recovered to almost the initial level. After precipitation with methyl acetate and dispersion of the PEAB-treated QDs in toluene, 5 μ L of NaBr solution in DMF was added to the QD solution, and mixed vigorously. The excess NaBr salt was removed in the same manner as PEAB. After repeating the addition of NaBr solution and removal of excess NaBr, the final NaBrpassivated QDs were recovered by precipitation with methyl acetate and redispersed in toluene.

Preparation of 2D Close-Packed Arrays of QDs. The 2D close-packed arrays of the QDs were formed directly on a TEM grid for both TEM imaging and spectroscopic measurements. To prepare the array sample, the concentrations of the QD solutions were adjusted to have an absorbance of ~30 at 400 nm for a 1 cm path length. On a

carbon-supported copper TEM grid 25 μ L of the QD solution in the mixture of toluene and hexane was drop-cast, and the sample was left under ambient conditions for 5 min for the solvent to evaporate. TEM images of the close-packed 2D arrays of the QDs were acquired using the FEI Tecnai G2 F20 ST field-emission TEM (FE-TEM) at 200 kV.

Optical Measurements. Steady-state absorption and PL spectra of the solutions of QD samples were obtained with an Ocean Optics USB spectrometer (USB2000 and QE65). The PL spectra of the 2D arrays of QDs on the TEM grid were obtained with a CCD camera (Princeton Instruments, ProEM+) and an imaging spectrograph (Princeton Instruments, Acton SpectraPro SP-2300) under excitation at 390 nm under ambient conditions. Temperature-dependent steadystate time-resolved PL spectra of the 2D arrays of QDs on the TEM grids were obtained using an open-cycle cryostat (Oxford Instruments Microstat-HE) in conjunction with a home-built microscope. The samples were excited with a 405 nm pulsed diode laser (Horiba, 45 ps pulse width). Except the data shown in Figure 4e, steady-state PL spectra of the samples in the cryostat were obtained using a CCD camera (Andor, iXon) coupled to an imaging spectrograph (Andor, Kymera 328i). PL spectra in Figure 4e were obtained with a combination of a different spectrograph (Princeton Instruments, Acton MicroSpec 2150i) and a CCD camera (Princeton Instruments, PIXIS 100) using another open-cycle cryostat (Janis ST-500). Timeresolved PL intensities of the arrays of 4.2 nm QDs (Figure S9) at 5 K were obtained using a 405 nm, 150 ns pulsed LED as the excitation source and time-correlated single photon counting (PicoHarp 300) with an avalanche photodiode (MPD PDM series) for detection.

■ RESULTS AND DISCUSSION

To investigate the effect of electronic coupling on the PL of bright and dark excitons in strongly quantum-confined CsPbBr₃ QDs, the original surface ligand (OLAB) was replaced with NaBr following the recently reported procedure, ²⁷ as detailed in the Experimental Section. This replacement was necessary to reduce the facet-to-facet distance of the QDs of the cube morphology from ~3 nm to the subnanometer regime, allowing for the overlap of the exciton wave function. Figure 1 shows the absorption and emission spectra

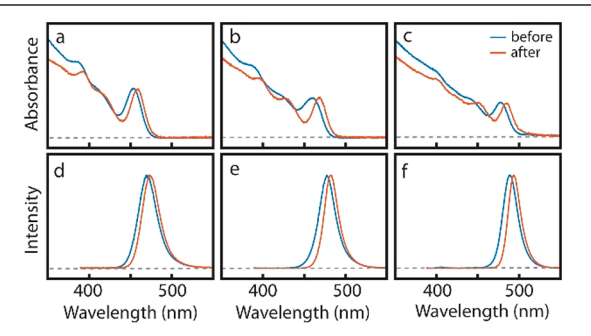


Figure 1. (a-c) Solution-phase absorption and (d-f) PL spectra of CsPbBr₃ QDs before (blue) and after (red) the ligand exchange from OLAB to NaBr. The sizes of the QDs after the ligand exchange, as determined from the size-dependent exciton PL peak, were (a, d) 3.8, (b, e) 4.2, and (c, f) 5.3 nm.

of CsPbBr₃ QDs of several different sizes dispersed in hexane in the strongly confined regime before and after the ligand replacement from OLAB to NaBr. For QDs of all sizes, a small redshift of the exciton peaks and the narrowing of their line width were observed after the ligand exchange. However, this is considered to be mainly from the additional size selection or minor surface reconstruction during the ligand exchange and the purification process rather than the intrinsic effects of putting different ligand on the QD surface. This is because NaBr should not spatially expand the electron or hole wave

functions, in contrast to some organic ligands known to spatially delocalize the wave function, which results in the redshift of the exciton transition. The negligible difference in the effects of OLAB and NaBr on the PL spectra was further confirmed by comparing the PL spectra of the CsPbBr₃ QDs ligand-exchanged with NaBr and OLAB using the same batch of the ligand-stripped QDs. The evolution of the PL spectra at each stage of the ligand exchange process is shown in Figure S1 of the Supporting Information. In this work, we used pairs of OLAB- and NaBr-passivated QDs with closely matching exciton PL spectra, which were chosen from multiple batches of QD samples rather than a direct comparison with the samples shown in Figure 1, to study the effects of electronic coupling.

Figure 2 shows the TEM images of OLAB- and NaBrpassivated QDs of three different sizes in the strongly confined

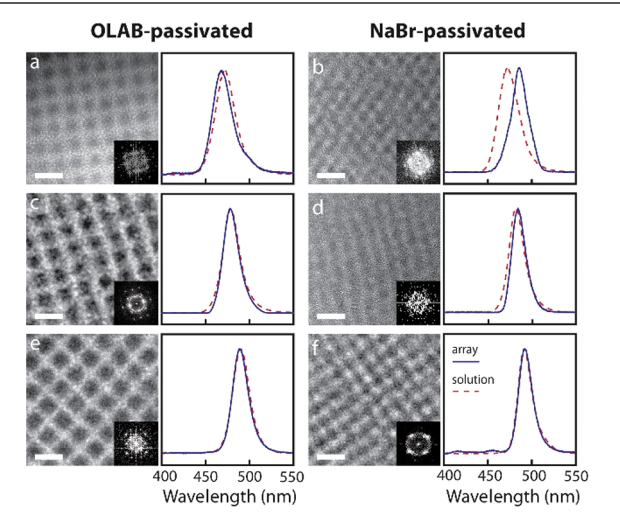


Figure 2. TEM images and room-temperature PL spectra of the 2D arrays of CsPbBr₃ QDs passivated with (a, c, and e) OLAB and (b, d, and f) NaBr formed on the TEM grids. PL spectra of the QD solution samples (dashed) are also shown for comparison. Sizes of the QDs and the PL peak position are shown in Table 1. The inset in each TEM image is the Fourier transform of the image. The scale bar represents 10 nm.

regime in addition to the PL spectra of the close-packed arrays of these QDs at room temperature. TEM images show well-ordered arrays of both OLAB- and NaBr-passivated QDs, and a survey of large area on the TEM grid indicates that 2D close-packing of the QDs occurs on the length scale of several hundred nanometer or larger; grain boundaries are present. (Figure S2). The PL spectra were recorded on an optical microscope under ambient conditions directly from the TEM

grids with the close-packed arrays of QDs following the weak cw excitation at 390 nm. The area on the TEM grid where the PL was measured was approximately $4 \times 4 \mu m^2$, which would contain multiple islands of 2D arrays of QDs. As a reference for comparison, the solution-phase PL spectra of the corresponding QD samples dispersed in hexane are also shown (dashed curve). Table 1 summarizes the PL peak positions from the QD solution samples and the arrays of QDs formed on the TEM grid. Center-to-center distances (d_{c-c}) of both OLABand NaBr-passivated QDs determined from the TEM images and their Fourier transforms are also compared. For all three different sizes, d_{c-c} decreases by 2.1-2.5 nm when OLAB is replaced with NaBr, resulting in a facet-to-facet distance of ~5 Å in the array of NaBr-passivated QDs. While thermally annealing the close-packed QD arrays generally makes the QDs closer, as evidenced by the increased electrical conductivity in earlier studies, 7,9 thermal annealing was avoided in this study to minimize the merging of the QDs and possible additional structural changes during heating.

The OLAB-passivated QDs show very similar PL spectra between the solution sample and the QD arrays on TEM grid; however, a small blueshift is noticeable for the smallest QDs (l = 3.8 nm), while the larger QDs show essentially identical PL spectra. In contrast, compared to the solution sample, the redshift of the 2D arrays of NaBr-passivated QDs increases as the size of the QDs decreases. The smallest NaBr-passivated QDs (l = 3.8 nm) exhibit a particularly large redshift of the PL (74 meV) in a close-packed array with respect to the solution phase, which is much larger than the 13 and 4 meV redshift observed in the QDs with l = 4.2 and 5.3 nm respectively. Compared to the close-packed array of OLAB-passivated QDs, the redshift exhibited by l = 3.8 nm QDs increases to 95 meV. The change in the dielectric environment was ruled out as being the cause for the large PL peak redshift of the QDs in the arrays. The PL spectra of 3.8 nm QDs in solvents with varied dielectric constants in the range of $\varepsilon = 1.9-5.6$ ($\varepsilon = 7.3$ for CsPbBr₃), which showed a much smaller PL redshift of less than 19 meV). (Figure S3). Typically, the redshift of the PL in the close-packed array of colloidal QDs has been explained by either electronic coupling between adjacent QDs or energy transfer between an energetically heterogeneous ensemble of the QDs. Both electronic coupling and energy transfer become more efficient as the interparticle distance decreases, which is qualitatively consistent with our observation. However, the redshift of the PL in the array of NaBr-passivated QDs in our study is largely attributed to electronic coupling facilitated by short facet-to-facet distance and strong quantum confinement, as will be discussed further below. Since the smallest QDs (l =3.8 nm) exhibit the largest redshift of the PL in the closepacked array, our discussion about the effect of electronic

Table 1. Center-to-Center Distance (d_{c-c}) between the QDs of Edge Length l Formed on the TEM Grid, PL Peak Wavelengths of the QD Arrays (λ_{array}) and QD Solution Samples (λ_{sol}) , and the PL Peak Redshift in the QD Array Referenced to the Solution Sample (ΔPL) in Figure 1

sample	ligand	1	d_{c-c}	$\lambda_{ m sol}$	$\lambda_{ m array}$	$\Delta ext{PL}$
a	OLAB	3.8 nm	6.8 nm	471.9 nm	468.1 nm	−21 meV
ь	NaBr		4.5 nm	472.0 nm	485.6 nm	74 meV
c	OLAB	4.2 nm	7.4 nm	478.6 nm	478.2 nm	−2 meV
d	NaBr		4.9 nm	481.8 nm	484.2 nm	13 meV
e	OLAB	5.3 nm	7.9 nm	490.2 nm	489.0 nm	-6 meV
f	NaBr		5.8 nm	491.2 nm	492.1 nm	4 meV

coupling on the bright and dark excitons in CsPbBr₃ QDs will focus more on l=3.8 nm QDs, which will be compared to the larger QDs (l=4.2 nm) that exhibit a much weaker effect. It is worth noting that the redshift of the PL in the array of l=3.8 nm NaBr-passivated QDs is also sensitive to the degree of order in the QD array, ²⁹ as more disorder in the QD array leads to a smaller PL redshift. (Figure S4). For the array of l=3.8 nm NaBr-passivated QDs that showed a regular ordered arrangement in the TEM image, the PL peak shift with respect to the solution PL (Δ PL) varied in the 45–74 meV range depending on the batches of QD used to form the arrays, potentially as a result of a small variation of the order or d_{c-c} .

One of the unique properties of exciton of the strongly quantum-confined CsPbBr3 QDs compared to their weakly and nonconfined counterparts is the accessibility to the lowestenergy dark exciton level, which exhibits intense and long-lived dark exciton PL.²⁶ Our recent studies of strongly confined CsPbBr₃ and CsPbI₃ QDs showed that increasing the quantum confinement resulted in a increased bright-dark energy splitting ($\Delta E_{\rm BD}$) and an increase in the dark exciton lifetime, which makes the dark exciton more readily accessible at higher temperatures.³⁰ To confirm that electronic coupling was the main cause of the PL redshift in the array of NaBr-passivated QDs and determine its effect on the exciton fine structure, specifically on the relative energetics and dynamics of bright and dark excitons, steady-state and time-dependent PL spectra were obtained for l = 3.8 nm QDs at various temperatures in the 5-300 K range. The PL spectra from the array of same-size OLAB-passivated QDs in which electronic coupling between the QDs was negligible were also obtained as references for the comparison.

First, we examined the dynamic PL spectra at 300 K, the point at which the bright exciton dominates the PL emission, using the QD arrays on a TEM grid placed in a vacuum cryostat. A 405 nm pulsed light (45 ps, 1 kHz) was used to excite the sample at a sufficiently low fluence (50 nJ/cm²) to ensure a very low excitation density ($\sim 5 \times 10^{-4}$ exciton/QD based on the reported absorption cross section of \sim 4.5 \times 10⁻¹⁵ cm²).³¹ To detect the time-dependent PL, a streak camera was used. Figure 3 shows the time-dependent PL spectra (panels a and b), time-dependent PL intensities (panels c and d), and time-dependent PL peak positions (panels e and f) of the arrays of OLAB- and NaBr-passivated QDs at 300 K. In the solution phase, these OLAB- and NaBr-passivated QDs exhibited similar PL peaks at 468.4 and 470.4 nm, respectively, as indicated by the dashed lines in Figure 3e and f. The line width of the solution-phase PL spectra is ~150 meV for both samples, indicating the similar ensemble heterogeneity. Note that the batch of the array of NaBr-passivated QDs used for the temperature-dependent measurement in the cryostat is different from that in Figure 2b measured under ambient conditions and ΔPL is smaller (45 meV) because of the batch-to-batch variation, as mentioned earlier.

The array of OLAB-passivated QDs exhibits almost single-exponential PL decay with the time constant of $\tau=4.2$ ns, which is close to that of the solution sample ($\tau=4-5$ ns). On the other hand, the array of NaBr-passivated QDs exhibits multiexponential decay comprised of a sub-nanosecond decay component ($\tau=0.42$ ns) that is absent in the solution PL and a slower decay component with an average time constant of $\tau=8.8$ ns. Earlier studies of QD solids and the chemically linked or directly bound QD dimer also reported the appearance of fast-decaying PL absent from the solution PL. 4,15,33,34 This was

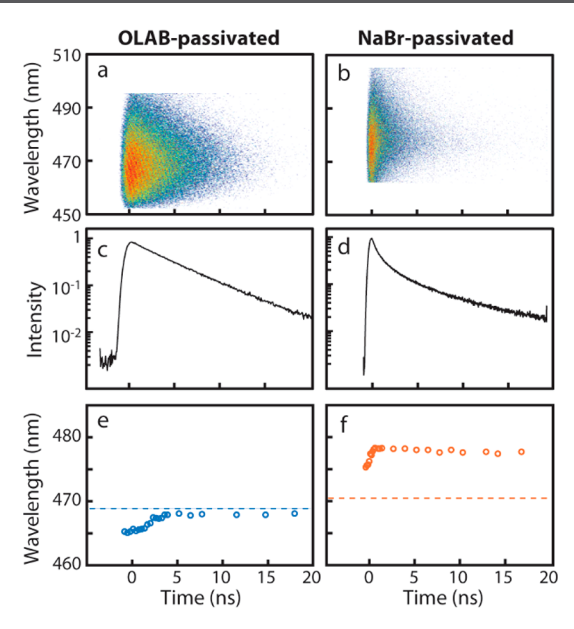


Figure 3. (a and b) Time-dependent PL spectra, (c and d) time-dependent PL intensities, and (e and f) time-dependent PL peak positions of the array of $CsPbBr_3$ QDs (l=3.8 nm) passivated with (a, c, and e) OLAB and (b, d, and f) NaBr at 300 K. Horizontal lines in panels e and f are the PL peak positions in solution.

explained as either energy transfer or charge transfer, which may also be possible in our sample. It is interesting to note that the slower decay time (8.8 ns) of the array of NaBr-passivated QDs, which accounts for the majority of photon emission, is slower than that of the solution sample (3–4 ns). We attribute this to the delocalization of electron and hole wave function to a larger volume because of electronic coupling, which slows the radiative recombination.

In Figure 3e and f, both OLAB- and NaBr-passivated QDs show a small dynamic redshift (~2.5 nm) during the early phase of the PL decay, which is absent in the PL of a dilute dispersion of QDs in polystyrene matrix. (Figure S5). It is notable that the dynamic redshift occurs on different time scales in the two QD samples, on ~4 ns and sub-nanosecond time scales for OLAB- and NaBr-passivated QDs, respectively. The dynamic redshift in the array of OLAB-passivated QDs can be interpreted as energy transfer between the nearby QDs, since such shift is absent in the dilute polymer dispersion of the QDs. The faster sub-nanosecond dynamic redshift in the array of NaBr-passivated QDs may also reflect the energy transfer between the QDs, which are more closely spaced than those in the array of OLAB-passivated QDs. In this interpretation, the same amount of dynamic redshift is consistent with the similar fwhm of the solution-phase PL at 300 K. While the relaxation within the manifold of the coupled states may be an alternative interpretation, the observed sub-nanosecond time scale of the redshift is much longer than typical relaxation in an electronic manifold coupled to phonon degrees of freedom (e.g., picoseconds).

Figure 4a shows the overview of the temperature-dependent steady-state PL spectra of the arrays of OLAB- and NaBr-passivated $l=3.8\,\mathrm{nm}$ QDs. A separate spectrometer operated in conjunction with a CCD camera was used for the steady-state PL measurement, as it provided a higher spectral resolution. As the temperature decreased, both OLAB- and NaBr-passivated QD arrays showed a redshift of the PL similar to those in previous reports on the temperature-dependent PL

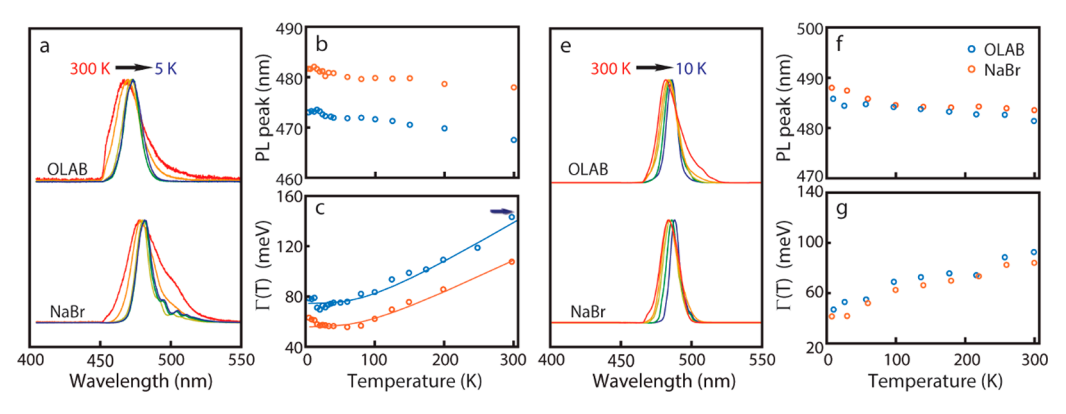


Figure 4. (a) Temperature-dependent PL spectra of CsPbBr₃ QDs (l = 3.8 nm) passivated with OLAB (top) and NaBr (bottom) ligands. From left to right, the temperatures are 300, 200, 150, 40, and 5 K. Part of the top spectra is cut off by a 450 nm long pass filter. (b) Temperature-dependent PL peak wavelength of OLAB- and NaBr-passivated QDs (l = 3.8 nm). (c) Temperature-dependent full-width at half-maximum ($\Gamma(T)$), of OLAB- and NaBr-passivated QDs (l = 3.8 nm). The solid curves are fit to $\Gamma(T)$, as discussed in the text. The arrow indicates $\Gamma(300 \text{ K})$ of the solution-phase PL for both QDs. (e) Temperature-dependent PL spectra of CsPbBr₃ QDs (l = 4.2 nm) passivated with OLAB (top) and NaBr (bottom) ligands. Form left to right, the temperatures are 300, 180, 100, 60, and 10 K. (f) Temperature-dependent PL peak wavelength of OLAB- and NaBr-passivated QDs (l = 4.2 nm). (g) Temperature-dependent $\Gamma(T)$ of OLAB- and NaBr-passivated QDs (l = 4.2 nm).

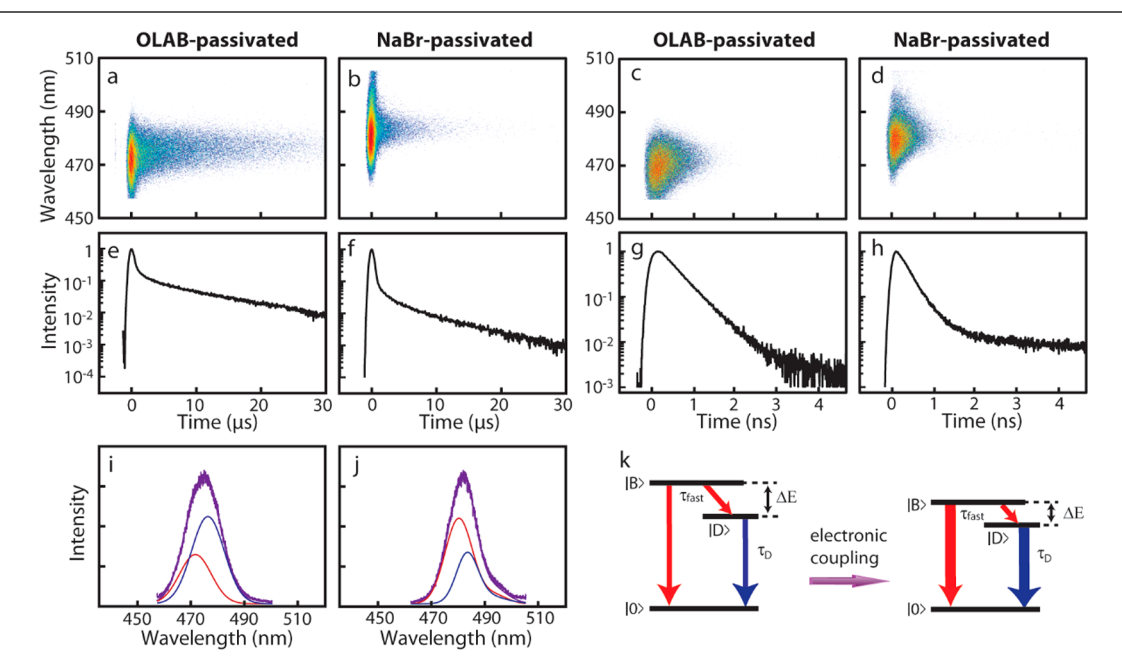


Figure 5. (a–d) Time-dependent PL spectra of the arrays of l = 3.8 nm CsPbBr₃ QDs passivated with (a and c) OLAB and (b and d) NaBr at 5 K in two different time windows. (e–h) Time-dependent PL intensities of the arrays of l = 3.8 nm CsPbBr₃ QDs passivated with (e and g) OLAB and (f and h) NaBr at 5 K in two different time windows. (i and j) PL spectra decomposed into the bright exciton (red) and dark exciton (blue) PL at 5 K shown in panels a and b. (k) Effect of electronic coupling on the decay and energetics of the bright and dark exciton PL and ΔE_{BD} .

of CsPbBr₃ QDs in the solution phase. The temperature-dependent PL peak shift is shown in Figure 4b. The broad shoulder near 500 nm in the PL spectrum of the array of NaBr-passivated QDs at 300 K in Figure 4a, which is absent in the array of OLAB-passivated QDs, was tentatively assigned to the merged QDs existing in the array. Below 100 K, this feature becomes more distinct and reveals multiple peaks, suggesting that there are several distinct merged QD species with larger effective sizes experiencing weaker quantum confinement. The three distinct side peaks in the 5 K spectrum of the NaBr-passivated QD array in Figure 4a are red-shifted by 70, 120, and 145 meV with respect to the main peak at 481.3 nm (Figure S6). They do not appear in the 5 K spectra of the arrays of 4.2 nm QDs passivated with either OLAB or NaBr, as shown in Figure 4e. This excludes the possibility of

phonon replica, ³⁹ which should exist in the QD arrays of all sizes regardless of the ligand. In contrast to the highly robust PL of the aged QDs in solution phase, which exhibited negligible change over the period of 1 year, the side peaks occurred only when NaBr-passivated QDs were made into the close-packed arrays (Figure S7), further supporting the merging scenario. In Figure 4c, when comparing the temperature-dependent fwhm of the PL spectra, $\Gamma(T)$, the contribution from the shoulder peaks was removed in the PL spectra of the array of NaBr-passivated QDs. Interestingly, in contrast to the solution PL spectra taken at 300 K that show a similar $\Gamma(300 \text{ K})$ value of ~150 meV for both QDs, the array of NaBr-passivated QDs exhibits a significantly smaller (20–40 meV) $\Gamma(T)$ value than the OLAB-passivated QDs over the entire range of temperatures.

Table 2. Parameters Extracted from 5 K PL Decay Data^a

ligand	$\lambda_{ m B}$	$\lambda_{ m D}$	$\Delta E_{ m BD}$	$I_{ m D}/I_{ m total}$	$ au_{ m D}$	$ au_{ m fast}$
OLAB	471.7 nm	476.4 nm	25 meV	65%	12 μs	0.42 ns
NaBr	480.3 nm	483.4 nm	16 meV	34%	9 us	0.29 ns

 $^a\lambda_{\rm B}$ and $\lambda_{\rm D}$ are PL wavelengths for bright and dark excitons, respectively; $\Delta E_{\rm BD}$ is bright—dark energy splitting; $au_{\rm D}$ and $au_{\rm fast}$ are the time constants for the dark exciton PL and the fast-decaying PL, respectively; and $I_{\rm D}/I_{\rm total}$ is the fraction of photons emitted from dark exciton in the total PL at 5 K.

In general, the decreasing PL line width would indicate weakening electron-phonon coupling for the noninteracting ensemble of QDs of a given static inhomogeneity. $\Gamma(T)$ is often analyzed using a model that includes the contributions from static inhomogeneity (Γ_{inh}) and coupling with acoustic phonon $(\gamma_{ac}T)$ and longitudinal optical (LO) phonon $(\gamma_{LO}N_{LO})$ modes, $\Gamma(T) = \gamma_{LO}N_{LO} + \gamma_{ac}T + \Gamma_{inh}$. 36 γ_{ac} and $\gamma_{\rm LO}$ represent the coupling strength to the acoustic phonon and the LO phonon, respectively. $N_{\rm LO}$ is the number of the LO phonon modes and is expressed $N_{LO} = 1/(\exp(E_{LO}/k_BT) - 1)$, where E_{LO} is LO phonon energy and k_B is the Boltzmann constant. Fitting the data in Figure 4c to $\Gamma(T)$ described above shows that γ_{LO} of the NaBr-passivated QDs is significantly smaller than that of the OLAB-passivated QDs (67 meV versus 86 meV, respectively), assuming the same γ_{ac} for both samples. (Figure S8) This indicates that the effect of electronic coupling in the 2D array of the QDs is phenomenologically equivalent to reducing the electron—phonon coupling when compared to that in the uncoupled QDs. While further study is needed to gain a more microscopic understanding of the narrowing of $\Gamma(T)$, we also note the similarity to the coupled molecular systems such as J aggregates, which exhibit a narrowing of the absorption line width or a narrowing of PL line width with super-radiant emission. 40,41 In contrast to l = 3.8 nm QDs, l =4.2 nm QDs that exhibit much weaker signs of electronic coupling in their PL spectra have much smaller differences in both the PL peak position and $\Gamma(T)$ between the arrays of OLAB- and NaBr-passivated QDs, as shown in Figure 4e-g. This indicates that narrowing of $\Gamma(T)$ observed in l=3.8 nm QDs in Figure 4c clearly correlates with the electronic coupling.

Figure 5 compares the time-dependent PL spectra (panel a d) and time-dependent PL intensity (panels e-h) of the arrays of OLAB- and NaBr-passivated l = 3.8 nm QDs at 5 K, which allows an examination of the effect of electronic coupling on the relative energy level and the dynamics of bright and dark excitons. To show the behavior of bright and dark exciton separately, the time-dependent PL are shown in two different time windows, namely, 30 μ s and 5 ns. Figure 5i and j are the time-integrated PL spectra and fit to the sum of the bright and dark exciton PL spectra for the arrays of OLAB- and NaBrpassivated QDs, respectively. At sufficiently low temperatures where the thermal energy (k_T) is much smaller than brightdark splitting energy ($\Delta E_{\rm BD}$), emission from the dark exciton level can be readily observed due to the suppression of thermal excitation from the dark state to the bright state.²⁶ The timedependent PL spectra and PL intensity presented in Figure 5a, b, e, and f show that the dark exciton PL decays on a microsecond time scale (τ_D) , which is well-separated from the fast decay component (au_{fast}) attributed to the decay of the bright exciton PL. The fast decay component is more clearly visible in Figure 5c and d. $\tau_{\rm fast}$ has two contributions, one from the relaxation of the bright exciton and another from the bright-to-dark transition. Since τ_{fast} and τ_{D} differ by four

orders of magnitude, bright and dark exciton PL spectra can be readily separated by time-gating the PL, as shown in Figure 5i and j, from which $\Delta E_{\rm BD}$ can be extracted. In Figure 5j, the shoulder peak near 500 nm, which was assigned to merged QDs in the steady-state PL shown in Figure 4a, also appears but is less well-resolved than that in the steady-state PL spectra due to the difference in the spectral resolutions of the two spectrometers. Table 2 summarizes the values of $\Delta E_{\rm BD},\,\tau_{\rm D}$, and $\tau_{\rm fast}$ obtained from the data in Figure 5. The fraction of photons emitted from dark state in the overall PL $(I_{\rm D}/I_{\rm total})$ at 5 K was determined from the data in Figure 5e, f, i, and j and is also shown in Table 2.

As clearly demonstrated by the data obtained from Figure 5, the main effect of electronic coupling in the array of NaBrpassivated l = 3.8 nm QDs is the decrease in the values of $\Delta E_{\rm BD}$, $\tau_{\rm D}$, and $\tau_{\rm fast}$ compared to those of the array of OLABpassivated QDs. This contrasts with the behavior of the NaBrpassivated l = 4.2 nm QDs, which exhibit much weaker electronic coupling. For instance, $\tau_{\rm D}$ values of the arrays of OLAB- and NaBr-passivated l = 4.2 nm QDs are 8.4 and 8.1 μ s, respectively, showing the much smaller effect on the decay rate of the dark exciton compared to that in the l = 3.8 nm QDs. (Figure S9). In our recent study of the PL from noninteracting CsPbBr3 QDs of different sizes dispersed in a polymer matrix, ΔE_{BD} and au_{D} decreased as the QD size increased.³⁰ The weaker electron-hole exchange interaction in the less-confined QDs was considered to be responsible for the decrease in $\Delta E_{\rm BD}$ with the increase in the QD size.^{30,42} In the presence of perturbations that can mix bright and dark states in semiconductor QDs, such as spin-orbit coupling, surface or defect spins, and optical or acoustic phonons, the mixing of bright and dark states is expected to increase with the decrease in $\Delta E_{\rm BD}$. Therefore, the decrease of $\Delta E_{\rm BD}$ in the electronically coupled array of QDs can be interpreted as the result of an increase in the spatial extent of the electron and hole wave function via electronic coupling, which reduced the electron-hole exchange interaction. This suggests that changes in the relative energies of the bright and dark exciton levels can be explained by the delocalization of the exciton wave function via electronic coupling in the array of QDs, which is similar to the effects of increasing the QD size in a noninteracting ensemble. The decrease in $\tau_{\rm D}$ due to electronic coupling is also consistent with the smaller $\Delta E_{\rm BD}$ values observed in the larger noninteracting QDs. Previous studies showed an approximately linear slope of $\Delta E_{\rm BD}$ versus inverse volume for the cube-shaped perovskite QDs, which was consistent with the theoretical prediction. 30,42,46 $\Delta E_{\rm BD}$ was also found to decrease as the thickness of the nanoplatelets increased.⁴⁷ A direct comparison of the effect of the size increase in uncoupled QDs and the delocalization of excitons limited to the lateral direction in a 2D array of the coupled QDs will not be quantitatively valid. However, comparing these data the sizedependent $\Delta E_{\rm BD}$ values reported in ref 30 indicates that the

change of $\Delta E_{\rm BD}$ observed in the coupled QDs in this study is equivalent to a volume increase of ~50% in uncoupled QDs.

It is interesting to note that τ_{fast} at 5 K is smaller in NaBrpassivated QDs than OLAB-passivated QDs, which contrasts with the bright exciton relaxation on a nanosecond time scale at 300 K in NaBr-passivated QDs ($\tau = 8.8$ ns) being slower than that in OLAB-passivated QDs (τ = 4.2 ns), as shown in Figure 3. τ_{fast} at 5 K reflects the time constant for the combined processes of bright exciton relaxation and the bright-dark transition. Therefore, the shortening of $au_{\rm fast}$ in NaBrpassivated QDs can have multiple contributions. While the PL quantum yield at 5 K is uncertain due to the difficulty of accurately quantifying the PL intensity from the QD arrays assembled on a TEM grid in vacuum, we consider the contribution from the nonradiative decay to be minimal at this low temperature. Since the PL from dark exciton with $\sim 10 \ \mu s$ can be readily observed and the relative PL intensity increases as the temperature decreases (Figure S10), we believe that the thermally activated trapping of an exciton, which leads to nonradiative decay, is effectively suppressed at 5 K. Under the assumption that excludes the nonradiative decay pathways of exciton, one possible contribution to the shortening of τ_{fast} is the giant oscillator strength transition effect that accelerates the bright exciton emission. A recent study of perovskite nanocrystals indicated that faster radiative recombination of the bright exciton is expected at lower temperatures due to the giant oscillator strength transition of the exciton, which is more prominent in the larger and less confined QDs. 48 An increase in the exciton oscillator strength upon cooling via the coherent center-of-mass delocalization of the exciton due to the giant oscillator transition strength effect has also been reported in CdSe nanoplatelets. 41 The effect of electronic coupling in the 2D array of the QDs on the temperature-dependent oscillator strength may be similar to that of increasing the size of the QDs. Presently, such a possibility cannot be directly confirmed using the temperature-dependent absorption spectra due to the difficulty of measuring the absorption from a 2D array of QDs. However, studies in the coupled 3D superlattice, whose temperature-dependent absorption may be easier to quantify, could shed more light on this issue. In addition, whether the electronic coupling will affect the bright-dark transition rate is another remaining question that will require further study.

CONCLUSION

In conclusion, we investigated the effects of electronic coupling between strongly quantum confined CsPbBr₃ QDs on the energetics and dynamics of bright and dark excitons. For this purpose, close-packed 2D arrays of QDs with a reduced facetto-facet distance of several angstroms were prepared via ligand replacement from OLAB to NaBr. Comparing the steady-state and time-dependent PL spectra of the arrays of OLAB- and NaBr-passivated QDs in a wide range of temperatures showed that bright-dark energy splitting decreases compared to that in the noninteracting array of the QDs. Additionally, there are redshifts of both the bright and dark levels. The dynamics of bright and dark exciton relaxation at 5 K also accelerates in the electronically coupled array of the QDs. These observations are consistent with the delocalization of the exciton wave function beyond a single QD in the coupled ensemble of the QDs, where the net effect is similar to increasing the volume of the noninteracting QDs.

ASSOCIATED CONTENT

Supporting Information

The Supporting Information is available free of charge at https://pubs.acs.org/doi/10.1021/acs.chemmater.2c00683.

Details of the additional experimental results, additional TEM images and optical spectra of QD arrays, and kinetic modeling of bright and dark exciton decay (PDF)

AUTHOR INFORMATION

Corresponding Author

Dong Hee Son — Department of Chemistry, Texas A&M University, College Station, Texas 77843, United States; Center for Nanomedicine, Institute for Basic Science and Graduate Program of Nano Biomedical Engineering, Advanced Science Institute, Yonsei University, Seoul 03722, Republic of Korea; ◎ orcid.org/0000-0001-9002-5188; Email: dhson@chem.tamu.edu

Authors

Xueting Tang — Department of Chemistry, Texas A&M University, College Station, Texas 77843, United States Daniel Rossi — Center for Nanomedicine, Institute for Basic Science and Graduate Program of Nano Biomedical Engineering, Advanced Science Institute, Yonsei University, Seoul 03722, Republic of Korea

Jinwoo Cheon – Center for Nanomedicine, Institute for Basic Science and Graduate Program of Nano Biomedical Engineering, Advanced Science Institute, Yonsei University, Seoul 03722, Republic of Korea; Orcid.org/0000-0001-8948-5929

Complete contact information is available at: https://pubs.acs.org/10.1021/acs.chemmater.2c00683

Notes

The authors declare no competing financial interest.

ACKNOWLEDGMENTS

This research was supported by National Science Foundation (CHE-2003961) and X-grants from Texas A&M University. J.C. acknowledges the Institute for Basic Science (IBS-R026-D1) for the support. X.T. acknowledges Mohit Khurana, Lanyin Luo, and Lok Raj Pant for their help with the acquisition of time-resolved PL intensity and temperature-dependent PL spectra of the 4.2 nm QDs.

■ REFERENCES

- (1) Kagan, C. R.; Lifshitz, E.; Sargent, E. H.; Talapin, D. V. Building devices from colloidal quantum dots. *Science* **2016**, 353 (6302), eaac 5523
- (2) Kagan, C. R.; Murray, C. B. Charge transport in strongly coupled quantum dot solids. *Nat. Nanotechnol.* **2015**, *10* (12), 1013–26.
- (3) Artemyev, M. V.; Bibik, A. I.; Gurinovich, L. I.; Gaponenko, S. V.; Woggon, U. Evolution from individual to collective electron states in a dense quantum dot ensemble. *Phys. Rev. B* **1999**, *60* (3), 1504–1506.
- (4) Koole, R.; Liljeroth, P.; de Mello Donega, C.; Vanmaekelbergh, D.; Meijerink, A. Electronic coupling and exciton energy transfer in CdTe quantum-dot molecules. *J. Am. Chem. Soc.* **2006**, *128* (32), 10436–41.
- (5) Artemyev, M. V.; Woggon, U.; Jaschinski, H.; Gurinovich, L. I.; Gaponenko, S. V. Spectroscopic study of electronic states in an ensemble of close-packed CdSe nanocrystals. *J. Phys. Chem. B* **2000**, *104* (49), 11617–11621.

- (6) Williams, K. J.; Tisdale, W. A.; Leschkies, K. S.; Haugstad, G.; Norris, D. J.; Aydil, E. S.; Zhu, X. Y. Strong electronic coupling in two-dimensional assemblies of colloidal PbSe quantum dots. *ACS Nano* **2009**, *3* (6), 1532–8.
- (7) Law, M.; Luther, J. M.; Song, Q.; Hughes, B. K.; Perkins, C. L.; Nozik, A. J. Structural, optical, and electrical properties of PbSe nanocrystal solids treated thermally or with simple amines. *J. Am. Chem. Soc.* **2008**, *130* (18), 5974–85.
- (8) Thuy, U. T. D.; Thuy, P. T.; Liem, N. Q.; Li, L.; Reiss, P. Comparative photoluminescence study of close-packed and colloidal InP/ZnS quantum dots. *Appl. Phys. Lett.* **2010**, *96* (7), 073102.
- (9) Talapin, D. V.; Murray, C. B. PbSe nanocrystal solids for n- and p-channel thin film field-effect transistors. *Science* **2005**, *310* (5745), 86–9.
- (10) Yu, D.; Wang, C.; Guyot-Sionnest, P. n-Type conducting CdSe nanocrystal solids. *Science* **2003**, *300* (5623), 1277–80.
- (11) Lee, J. S.; Kovalenko, M. V.; Huang, J.; Chung, D. S.; Talapin, D. V. Band-like transport, high electron mobility and high photoconductivity in all-inorganic nanocrystal arrays. *Nat. Nanotechnol.* **2011**, *6* (6), 348–52.
- (12) Liu, Y.; Tolentino, J.; Gibbs, M.; Ihly, R.; Perkins, C. L.; Liu, Y.; Crawford, N.; Hemminger, J. C.; Law, M. PbSe quantum dot field-effect transistors with air-stable electron mobilities above 7 cm 2 V $^{-1}$ s $^{-1}$. *Nano Lett.* **2013**, *13* (4), 1578–87.
- (13) Lan, X.; Chen, M.; Hudson, M. H.; Kamysbayev, V.; Wang, Y.; Guyot-Sionnest, P.; Talapin, D. V. Quantum dot solids showing stateresolved band-like transport. *Nat. Mater.* **2020**, *19* (3), 323–329.
- (14) Crisp, R. W.; Schrauben, J. N.; Beard, M. C.; Luther, J. M.; Johnson, J. C. Coherent exciton delocalization in strongly coupled quantum dot arrays. *Nano Lett.* **2013**, *13* (10), 4862–9.
- (15) Cui, J.; Panfil, Y. E.; Koley, S.; Shamalia, D.; Waiskopf, N.; Remennik, S.; Popov, I.; Oded, M.; Banin, U. Colloidal quantum dot molecules manifesting quantum coupling at room temperature. *Nat. Commun.* **2019**, *10*, 5401.
- (16) Panfil, Y. E.; Shamalia, D.; Cui, J.; Koley, S.; Banin, U. Electronic coupling in colloidal quantum dot molecules; the case of CdSe/CdS core/shell homodimers. *J. Chem. Phys.* **2019**, *151* (22), 224501.
- (17) Fan, J. Z.; Vafaie, M.; Bertens, K.; Sytnyk, M.; Pina, J. M.; Sagar, L. K.; Ouellette, O.; Proppe, A. H.; Rasouli, A. S.; Gao, Y.; Baek, S. W.; Chen, B.; Laquai, F.; Hoogland, S.; Arquer, F. P. G.; Heiss, W.; Sargent, E. H. Micron Thick Colloidal Quantum Dot Solids. *Nano Lett.* **2020**, *20* (7), 5284–5291.
- (18) Jena, A. K.; Kulkarni, A.; Miyasaka, T. Halide Perovskite Photovoltaics: Background, Status, and Future Prospects. *Chem. Rev.* **2019**, *119* (5), 3036–3103.
- (19) Quan, L. N.; Rand, B. P.; Friend, R. H.; Mhaisalkar, S. G.; Lee, T. W.; Sargent, E. H. Perovskites for Next-Generation Optical Sources. *Chem. Rev.* **2019**, *119* (12), 7444–7477.
- (20) Tong, Y.; Yao, E. P.; Manzi, A.; Bladt, E.; Wang, K.; Doblinger, M.; Bals, S.; Muller-Buschbaum, P.; Urban, A. S.; Polavarapu, L.; Feldmann, J. Spontaneous Self-Assembly of Perovskite Nanocrystals into Electronically Coupled Supercrystals: Toward Filling the Green Gap. *Adv. Mater.* **2018**, *30* (29), No. 1801117.
- (21) van der Burgt, J. S.; Geuchies, J. J.; van der Meer, B.; Vanrompay, H.; Zanaga, D.; Zhang, Y.; Albrecht, W.; Petukhov, A. V.; Filion, L.; Bals, S.; Swart, I.; Vanmaekelbergh, D. Cuboidal Supraparticles Self-Assembled from Cubic CsPbBr₃ Perovskite Nanocrystals. *J. Phys. Chem. C* **2018**, *122* (27), 15706–15712.
- (22) Imran, M.; Ijaz, P.; Baranov, D.; Goldoni, L.; Petralanda, U.; Akkerman, Q.; Abdelhady, A. L.; Prato, M.; Bianchini, P.; Infante, I.; Manna, L. Shape-Pure, Nearly Monodispersed CsPbBr₃ Nanocubes Prepared Using Secondary Aliphatic Amines. *Nano Lett.* **2018**, *18* (12), 7822–7831.
- (23) Raino, G.; Becker, M. A.; Bodnarchuk, M. I.; Mahrt, R. F.; Kovalenko, M. V.; Stoferle, T. Superfluorescence from lead halide perovskite quantum dot superlattices. *Nature* **2018**, *563* (7733), *671*–675.

- (24) Baranov, D.; Toso, S.; Imran, M.; Manna, L. Investigation into the Photoluminescence Red Shift in Cesium Lead Bromide Nanocrystal Superlattices. *J. Phys. Chem. Lett.* **2019**, *10* (3), 655–660.
- (25) Dong, Y.; Qiao, T.; Kim, D.; Parobek, D.; Rossi, D.; Son, D. H. Precise Control of Quantum Confinement in Cesium Lead Halide Perovskite Quantum Dots via Thermodynamic Equilibrium. *Nano Lett.* **2018**, *18* (6), 3716–3722.
- (26) Rossi, D.; Liu, X.; Lee, Y.; Khurana, M.; Puthenpurayil, J.; Kim, K.; Akimov, A. V.; Cheon, J.; Son, D. H. Intense Dark Exciton Emission from Strongly Quantum-Confined CsPbBr₃ Nanocrystals. *Nano Lett.* **2020**, 20 (10), 7321–7326.
- (27) Dong, Y.; Wang, Y. K.; Yuan, F.; Johnston, A.; Liu, Y.; Ma, D.; Choi, M. J.; Chen, B.; Chekini, M.; Baek, S. W.; Sagar, L. K.; Fan, J.; Hou, Y.; Wu, M.; Lee, S.; Sun, B.; Hoogland, S.; Quintero-Bermudez, R.; Ebe, H.; Todorovic, P.; Dinic, F.; Li, P.; Kung, H. T.; Saidaminov, M. I.; Kumacheva, E.; Spiecker, E.; Liao, L. S.; Voznyy, O.; Lu, Z. H.; Sargent, E. H. Bipolar-shell resurfacing for blue LEDs based on strongly confined perovskite quantum dots. *Nat. Nanotechnol.* **2020**, *15* (8), 668–674.
- (28) Harris, R. D.; Bettis Homan, S.; Kodaimati, M.; He, C.; Nepomnyashchii, A. B.; Swenson, N. K.; Lian, S.; Calzada, R.; Weiss, E. A. Electronic Processes within Quantum Dot-Molecule Complexes. *Chem. Rev.* **2016**, *116* (21), 12865–12919.
- (29) Yang, J.; Wise, F. W. Effects of Disorder on Electronic Properties of Nanocrystal Assemblies. *J. Phys. Chem. C* **2015**, *119* (6), 3338–3347.
- (30) Rossi, D.; Qiao, T.; Liu, X.; Khurana, M.; Akimov, A. V.; Cheon, J.; Son, D. H. Size-dependent dark exciton properties in cesium lead halide perovskite quantum dots. *J. Chem. Phys.* **2020**, *153* (18), 184703.
- (31) Puthenpurayil, J.; Cheng, O. H.; Qiao, T.; Rossi, D.; Son, D. H. On the determination of absorption cross section of colloidal lead halide perovskite quantum dots. *J. Chem. Phys.* **2019**, *151* (15), 154706.
- (32) Rossi, D.; Wang, H.; Dong, Y.; Qiao, T.; Qian, X.; Son, D. H. Light-Induced Activation of Forbidden Exciton Transition in Strongly Confined Perovskite Quantum Dots. *ACS Nano* **2018**, *12* (12), 12436–12443.
- (33) Kagan, C. R.; Murray, C. B.; Bawendi, M. G. Long-range resonance transfer of electronic excitations in close-packed CdSe quantum-dot solids. *Phys. Rev. B: Condens. Matter* **1996**, *54* (12), 8633–8643.
- (34) Crooker, S. A.; Hollingsworth, J. A.; Tretiak, S.; Klimov, V. I. Spectrally resolved dynamics of energy transfer in quantum-dot assemblies: towards engineered energy flows in artificial materials. *Phys. Rev. Lett.* **2002**, *89* (18), 186802.
- (35) Diroll, B. T.; Zhou, H.; Schaller, R. D. Low-Temperature Absorption, Photoluminescence, and Lifetime of CsPbX₃ (X = Cl, Br, I) Nanocrystals. *Adv. Funct. Mater.* **2018**, 28 (30), 1800945.
- (36) Cheng, O. H.; Qiao, T.; Sheldon, M.; Son, D. H. Size- and temperature-dependent photoluminescence spectra of strongly confined CsPbBr₃ quantum dots. *Nanoscale* **2020**, *12* (24), 13113–13118.
- (37) Hudait, B.; Dutta, S. K.; Patra, A.; Nasipuri, D.; Pradhan, N. Facets Directed Connecting Perovskite Nanocrystals. *J. Am. Chem. Soc.* **2020**, *142* (15), 7207–7217.
- (38) Nagaoka, Y.; Hills-Kimball, K.; Tan, R.; Li, R.; Wang, Z.; Chen, O. Nanocube Superlattices of Cesium Lead Bromide Perovskites and Pressure-Induced Phase Transformations at Atomic and Mesoscale Levels. *Adv. Mater.* (Weinheim, Ger.) 2017, 29 (18), 1606666.
- (39) Iaru, C. M.; Geuchies, J. J.; Koenraad, P. M.; Vanmaekelbergh, D.; Silov, A. Y. Strong Carrier-Phonon Coupling in Lead Halide Perovskite Nanocrystals. *ACS Nano* **2017**, *11* (11), 11024–11030.
- (40) Potma, E. O.; Wiersma, D. A. Exciton superradiance in aggregates: The effect of disorder, higher order exciton-phonon coupling and dimensionality. *J. Chem. Phys.* **1998**, *108* (12), 4894–4903.

- (41) Wubs, M.; Knoester, J. Exchange narrowing in dynamically disordered molecular aggregates. *Chem. Phys. Lett.* **1998**, 284 (1–2), 63–70.
- (42) Leung, K.; Pokrant, S.; Whaley, K. B. Exciton fine structure in CdSe nanoclusters. *Phys. Rev. B* **1998**, *57* (19), 12291–12301.
- (43) Rodina, A.; Efros, A. L. Magnetic Properties of Nonmagnetic Nanostructures: Dangling Bond Magnetic Polaron in CdSe Nanocrystals. *Nano Lett.* **2015**, *15* (6), 4214–22.
- (44) Rodina, A. V.; Efros, A. L. Radiative recombination from dark excitons in nanocrystals: Activation mechanisms and polarization properties. *Phys. Rev. B* **2016**, 93 (15), 155427.
- (45) Oron, D.; Aharoni, A.; de Mello Donega, C.; van Rijssel, J.; Meijerink, A.; Banin, U. Universal role of discrete acoustic phonons in the low-temperature optical emission of colloidal quantum dots. *Phys. Rev. Lett.* **2009**, *102* (17), 177402.
- (46) Sercel, P. C.; Lyons, J. L.; Wickramaratne, D.; Vaxenburg, R.; Bernstein, N.; Efros, A. L. Exciton Fine Structure in Perovskite Nanocrystals. *Nano Lett.* **2019**, *19* (6), 4068–4077.
- (47) Gramlich, M.; Swift, M. W.; Lampe, C.; Lyons, J. L.; Doblinger, M.; Efros, A. L.; Sercel, P. C.; Urban, A. S. Dark and Bright Excitons in Halide Perovskite Nanoplatelets. *Adv. Sci.* **2022**, *9* (5), No. 2103013.
- (48) Becker, M. A.; Vaxenburg, R.; Nedelcu, G.; Sercel, P. C.; Shabaev, A.; Mehl, M. J.; Michopoulos, J. G.; Lambrakos, S. G.; Bernstein, N.; Lyons, J. L.; Stoferle, T.; Mahrt, R. F.; Kovalenko, M. V.; Norris, D. J.; Raino, G.; Efros, A. L. Bright triplet excitons in caesium lead halide perovskites. *Nature* **2018**, *553* (7687), 189–193.

☐ Recommended by ACS

Coupling Perovskite Quantum Dot Pairs in Solution using a Nanoplasmonic Assembly

Hao Zhang, Reuven Gordon, et al.

JUNE 29, 2022 NANO LETTERS

READ 🗹

Excited-State Properties of Defected Halide Perovskite Quantum Dots: Insights from Computation

Carlos Mora Perez, Amanda J. Neukirch, et al.

JANUARY 20, 2021

THE JOURNAL OF PHYSICAL CHEMISTRY LETTERS

READ 🗹

Complete Mapping of Interacting Charging States in Single Coupled Colloidal Quantum Dot Molecules

Yossef E. Panfil, Uri Banin, et al.

MARCH 15, 2022 ACS NANO

READ 🗹

Purcell Enhancement and Wavelength Shift of Emitted Light by CsPbI₃ Perovskite Nanocrystals Coupled to Hyperbolic Metamaterials

Hamid Pashaei Adl, Juan P. Martínez-Pastor, et al.

OCTOBER 26, 2020

ACS PHOTONICS

READ 🗹

Get More Suggestions >